Monthly Notices
of the
ROYAL ASTRONOMICAL SOCIETY

MNRAS **428,** 834–844 (2013) doi:10.1093/mnras/sts082

The *Herschel* Fornax Cluster Survey – I. The bright galaxy sample

J. I. Davies,[1]⋆ S. Bianchi,[2] M. Baes,[3] A. Boselli,[4] L. Ciesla,[4] M. Clemens,[5] T. A. Davis,[6] I. De Looze,[3] S. di Serego Alighieri,[2] C. Fuller,[1] J. Fritz,[3] L. K. Hunt,[2] P. Serra,[7] M. W. L. Smith,[1] J. Verstappen,[3] C. Vlahakis,[8] E. M. Xilouris,[9] D. Bomans,[10] T. Hughes,[11] D. Garcia-Appadoo[8] and S. Madden[12]

[1]*School of Physics and Astronomy, Cardiff University, The Parade, Cardiff CF24 3AA*
[2]*INAF–Osservatorio Astrofisico di Arcetri, Largo Enrico Fermi 5, I-50125 Firenze, Italy*
[3]*Sterrenkundig Observatorium, Universiteit Gent, KrijgslAAn 281 S9, B-9000 Gent, Belgium*
[4]*Laboratoire d'Astrophysique de Marseille, UMR 6110 CNRS, 38 rue F. Joliot-Curie, F-13388 Marseille, France*
[5]*INAF–Osservatorio Astronomico di Padova, Vicolo dell'Osservatorio 5, I-35122 Padova, Italy*
[6]*European Southern Observatory, Karl-Schwarzschild Str. 2, D-85748 Garching bei Muenchen, Germany*
[7]*Netherlands Institute for Radio Astronomy (ASTRON), Postbus 2, NL-7990 AA Dwingeloo, the Netherlands*
[8]*Joint ALMA Observatory (JAO), Vitacura, Santiago, Chile*
[9]*Institute for Astronomy, Astrophysics, Space Applications & Remote Sensing, National Observatory of Athens, P. Penteli, GR-15236 Athens, Greece*
[10]*Astronomical Institute, Ruhr-University Bochum, Universitaetsstr. 150, D-44780 Bochum, Germany*
[11]*Kavli Institute for Astronomy & Astrophysics, Peking University, Beijing 100871, China*
[12]*Laboratoire AIM, CEA/DSM–CNRS–Université Paris Diderot, Irfu/Service, Paris, France*

Accepted 2012 September 25. Received 2012 September 24; in original form 2012 August 6

ABSTRACT

We present *Herschel* Space Telescope observations of the nearby Fornax cluster at 100, 160, 250, 350 and 500 μm with a spatial resolution of 7–36 arcsec (10 arcsec ≈ 1 kpc at $d_{\rm Fornax}$ = 17.9 Mpc). We define a sample of 11 bright galaxies, selected at 500 μm, that can be directly compared with our past work on the Virgo cluster. We check and compare our results with previous observations made by *IRAS* and *Planck*, finding good agreement. The far-infrared luminosity density is higher, by about a factor of 3, in Fornax compared to Virgo, consistent with the higher number density of galaxies. The 100 μm (42.5–122.5 μm) luminosity is two orders of magnitude larger in Fornax than in the local field as measured by *IRAS*. We calculate stellar ($L_{0.4-2.5}$) and far-infrared ($L_{100-500}$) luminosities for each galaxy and use these to estimate a mean optical depth of $\tau = 0.4 \pm 0.1$ – the same value as we previously found for Virgo cluster galaxies. For 10 of the 11 galaxies (NGC 1399 excepted), we fit a modified blackbody curve ($\beta = 2.0$) to our observed flux densities to derive dust masses and temperatures of $10^{6.54-8.35}$ $M_\odot$ and T =14.6–24.2 K, respectively, values comparable to those found for Virgo. The derived stars-to-gas(atomic) and gas(atomic)-to-dust ratios vary from 1.1–67.6 to 9.8–436.5, respectively, again broadly consistent with values for Virgo. Fornax is a mass overdensity in stars and dust of about 120 when compared to the local field (30 for Virgo). Fornax and Virgo are both a factor of 6 lower overdensities in gas(atomic) than in stars and dust indicating loss of gas, but not dust and stars, in the cluster environment. We consider in more detail two of the sample galaxies. As the brightest source in either Fornax or Virgo, NGC 1365 is also detected by *Planck*. The *Planck* data fit the PACS/SPIRE spectral energy distribution out to 1382 μm with no evidence of other sources of emission ('spinning dust', free–free, synchrotron). At the opposite end of the scale, NGC 1399 is detected only at 500 μm with the emission probably arising from the nuclear radio source rather than interstellar dust.

Key words: Galaxies: clusters individual: Fornax – Galaxies: ISM.

1 INTRODUCTION

The two nearest galaxy clusters to us are Virgo and Fornax. The NASA Extragalactic Database (NED) gives the distance of M87

⋆E-mail: jid@astro.cf.ac.uk

(the giant elliptical at the heart of Virgo) as 16.8 Mpc, while the similar galaxy at the heart of Fornax (NGC 1399) lies at 17.9 Mpc. Both clusters are at high galactic latitude ($b_{\rm Virgo} = 74.^{\circ}5$, $b_{\rm Fornax} = -53.^{\circ}6$) and so are ideal targets for extragalactic studies at all wavelengths. Virgo and Fornax were observed at optical wavelengths (photographic) in the 1980s leading to the most complete catalogues of cluster members (Binggeli et al. 1985; Ferguson 1989a). Fornax is somewhat less populous than Virgo with just 350 members listed in the Fornax Cluster Catalogue (FCC; Ferguson 1989a) compared to about 2000 in the Virgo Cluster Catalogue (VCC; Binggeli et al. 1985).

The Fornax cluster has a velocity dispersion of $\sim$370 km s^{-1} and a core radius of $0.^{\circ}7$ (250 kpc), which gives a mass of $\approx 7 \times 10^{13}$ M$_{\odot}$, about a factor of 7 less than Virgo (Jordan et al. 2007 and references therein) and so Fornax might also be described as a large group. Like Virgo, Fornax does show evidence of sub-structure indicating its current and continuing assembly (Drinkwater et al. 2001) though it is more regular in shape and probably more dynamically evolved than Virgo. Although less massive than Virgo, the central galaxy number density is about three times higher in Fornax than in Virgo and with its lower velocity dispersion we might expect more influential interactions of Fornax galaxies with one another. To quantify this the relaxation time of Fornax, a measure of the time-scale for gravitational interactions, is about one-third that of Virgo ($T_{\rm Relax}^{\rm Virgo} \approx 4 \times 10^{10}$ yr; Boselli & Gavazzi 2006). However, this time-scale is long compared to the crossing time which determines how long a mechanism like ram pressure stripping might be effective. The crossing time of Fornax and Virgo are about equal ($T_{\rm Cross}^{\rm Virgo} \approx 2 \times 10^{9}$ yr; Boselli & Gavazzi 2006), but the lower velocity dispersion of Fornax makes the intergalactic medium less influential for the same intergalactic medium density. We can quantify how 'effective' (E) ram pressure stripping might be using $E \propto t_{\rm Cross} \delta v^2 \rho_{\rm g}$ (Gunn & Gott 1972) where δv is the cluster velocity dispersion and $\rho_{\rm g}$ is the gas density. From the X-ray data (Schindler, Binggeli & Bohringer 1999; Paolillo et al. 2002; Scharf et al. 2005) the central gas density and velocity dispersion of Virgo is about four and two times higher, respectively, than Fornax making Virgo potentially about 16 times more 'effective' at ram pressure stripping. So, because of these diverse cluster properties Virgo and Fornax galaxies may have quite different gas accretion/stripping histories.

Our new observations of Fornax cluster galaxies described below make use of the unique imaging qualities and sensitivity of the *Herschel* Space Telescope at five wavelengths from 100 to 500 μm. With a 3.5 m mirror, the spatial resolution of *Herschel* at these wavelengths ranges from 7 to 36 arcsec, enabling spatially resolved observations of many of the bright galaxies at the distance of Fornax (10 arcsec $\equiv$ 1 kpc).

The *Herschel* Fornax Cluster Survey (HeFoCS) is an ESA *Herschel* Space Observatory (Pilbratt et al. 2010) Open Time Project. The project was awarded 31 h of observing time in parallel mode using PACS (Poglitsch et al. 2010) at 100 and 160 μm, and SPIRE (Griffin et al. 2010) at 250, 350 and 500 μm. Pre-*Herschel* comparable surveys describing the far-infrared properties of nearby bright galaxies in both cluster and field have been described by Soifer et al. (1987), Doyon & Joseph (1989, *IRAS*), Tuffs et al. (2002, *ISO*), Draine et al. (2007, *Spitzer*). Davies et al. (2012) have presented *Herschel* observations of the bright galaxies in the Virgo cluster.

In this paper, we describe the first results from our Fornax cluster survey concentrating on the properties of the bright galaxies that are detected at high signal-to-noise ratio. In many ways this paper is a continuation of the work we have previously done using the Herschel Virgo Cluster Survey (HeViCS) data, which is described in the following series of papers: Paper I (Davies et al. 2010) considered the properties of the bright galaxies in a single central 4×4 square degree HeViCS field, Paper II (Cortese et al. 2010) describes the truncation of cluster galaxy dust discs, Paper III (Clemens et al. 2010) on the dust lifetime in early-type galaxies, Paper IV (Smith et al. 2010) considers the spiral galaxy dust surface density and temperature distribution, Paper V (Grossi et al. 2010) on the properties of metal-poor star-forming dwarf galaxies, Paper VI (Baes et al. 2010) looks at the lack of thermal emission from the elliptical galaxy M87, Paper VII (De Looze et al. 2010) discusses the far-infrared detection of dwarf elliptical galaxies, Paper VIII (Davies et al. 2012) looks at the properties of the 78 brightest Virgo galaxies, Paper IX (Magrini et al. 2011) compares galactic metallicity and dust-to-gas ratio gradients, Paper X (Corbelli et al. 2012) considers the relationship between cold dust and molecular gas, Paper XI (Pappalardo et al. 2012) assesses the environmental effects on molecular gas and dust in spiral discs and Paper XII (Auld et al. 2012) discusses the detection of far-infrared emission from all catalogued VCC galaxies. A further paper (Boselli et al. 2010) discusses the spectral energy distributions (SEDs) of HeViCS galaxies together with others observed as part of the *Herschel* Reference Survey.

2 OBSERVATIONS, DATA REDUCTION, OBJECT SELECTION AND CALIBRATION CHECKS

We have obtained $\sim$16 square degrees of data from a single field centred on the central Fornax cluster galaxy NGC 1399 [RA (J2000) = $03^{\rm h}38^{\rm m}29.^{\rm s}08$, Dec. (J2000) = $-35^{\circ}27'2.''7$], Fig. 1. We use parallel mode and a fast scan rate of 60 arcsec s^{-1} (as used for the HeViCS data) over two×two orthogonal cross-linked scan directions (four scans).

PACS data reduction was carried out with the standard pipeline for both the 100 and 160 μm channels up to Level-1. The four scans were then combined and maps made using the *Scanamorphos* map maker (Roussel 2012). We chose to use *Scanamorphos*, instead of the phot-project mapper used in previous papers (Davies et al. 2012), as this avoids the necessity of high-pass filtering, which would remove the lower level extended emission. After combining orthogonal scans the full width at half-maximum (FWHM) beam sizes are approximately 7 and 13 arcsec with pixel sizes of 2 and 3 arcsec for the 100 and 160 μm channels, respectively.

The SPIRE data were also processed up to Level-1 with a custom-driven pipeline script adapted from the official pipeline (*POF5_pipeline.py*, dated 2010 June 8) as provided by the SPIRE Instrument Control Centre (ICC).[1] This JYTHON script was run in the *Herschel* Interactive Processing Environment (HIPE – Ott 2010). Our data reduction up to Level-1 is very similar to the *Herschel* Common Science System/Standard Product Generation v5 with a calibration based on Neptune data. Specific differences to the standard pipeline were that we used the *sigmaKappaDeglitcher* instead of the ICC-default *waveletDeglitcher*. Furthermore, we did not run the default *temperatureDriftCorrection* and the residual, median baseline subtraction. Instead, we use a custom method called BriGAdE (Smith et al., in preparation) to remove the temperature drift and bring all bolometers to the same level (equivalent to baseline removal).

[1] See 'The SPIRE Analogue Signal Chain and Photometer Detector Data Processing Pipeline' (Griffin et al. 2009) or Dowell et al. (2010) for a more detailed description of the pipeline and a list of the individual modules.

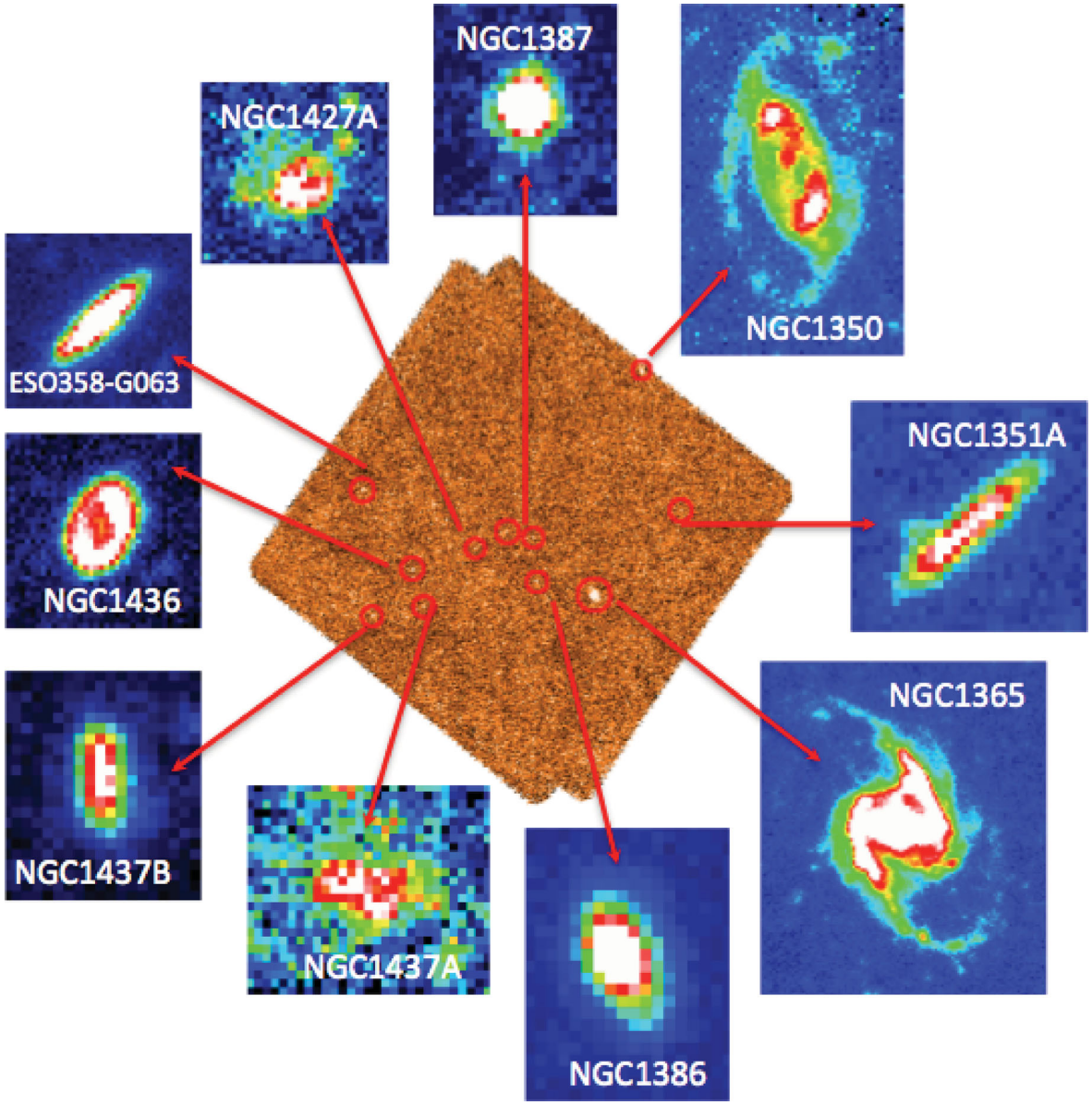

Figure 1. The HeFoCS 500 μm data with the positions and names of 10 of the 11 detected bright galaxies marked (the exception is NGC 1399, which is shown in more detail in Fig. 5). Insets are 250 μm images of 10 of the galaxies (NGC 1399 is not detected at 250 μm).

We have found that this method improves the baseline subtraction significantly especially in cases where there are strong temperature variations during the observation.

Scans were then combined to make our final maps using the naive mapper provided in the standard pipeline. The FWHM of the SPIRE beams are 18.2, 24.5 and 36.0 arcsec with pixel sizes of 6, 8 and 12 arcsec at 250, 350 and 500 μm, respectively. The beam areas used were 423, 751 and 1587 arcsec^2, respectively. The final data products have a 1σ noise, determined from the whole of each image, of ∼0.6, 0.7, 1.0, 1.0 and 1.0 mJy pixel^{-1} or 6.4, 3.3, 1.2, 0.7 and 0.3 MJ sr^{-1} at 100, 160, 250, 350 and 500 μm, respectively.

As in Davies et al. (2012) for the Virgo cluster we obtain a bright far-infrared selected sample by carrying out our initial object selection at 500 μm. This is because it is the least explored part of the spectrum, it has the lowest resolution and most galaxies will produce their lowest flux in this band, which should guarantee a detection in all five bands. To produce an objectively selected sample we used the automatic image detection algorithm SExtractor (Bertin & Arnouts 1996). To minimize background contamination by faint sources each object was required to have more than 41 connected pixels at 1.5σ_{500} or above.[2] The result is a 500 μm flux density limit of ∼0.1 Jy for sources with a diameter larger than 1.4 arcmin. Each object was then checked for correspondence with a known Fornax Cluster galaxy (FCC). The final sample consists of 11 Fornax Cluster objects, which is just 4 per cent of the 256 FCC galaxies in our field. This compares with 78 galaxies detected in just the same way in the Virgo cluster, which is 12 per cent of the galaxies in this area listed in the VCC (Davies et al. 2012). A more straight forward comparison is that 14 galaxies were detected in the central

[2] We used 30 connected pixels for the Virgo (HeViCS) data in Davies et al. (2012), but since then we have changed our pixel scale from 14 to 12 arcsec at 500 μm and so the two are equivalent.

16 square degree Virgo field centred on M87, compared to 11 over the same area centred on NGC 1399. Discarded objects are in the background of Fornax.

In the standard way the data were initially smoothed and re-gridded to the 500 μm resolution and pixel scale. Elliptical apertures were chosen by eye using the 500 μm data, with the sky defined by a concentric annulus. These same annuli were then used on the smoothed and re-gridded data at other wavelengths. As a test we compared this method with carrying out the aperture photometry on the original unsmoothed 100 μm data, our criteria being correspondence with the flux density values at 100 μm from *IRAS*. These tests showed that we obtained a much better result by using the original resolution data, rather than the smoothed and re-gridded data. So, independent measurements were carried out on the maps at the original resolution, defining by eye for each galaxy an elliptical aperture and a nearby sky aperture that avoided pixels contaminated by bright background sources. The flux densities quoted in Table 1 come from aperture photometry using this unsmoothed and original resolution data.

Flux density errors are estimated as in Davies et al. (2012). A large part of the uncertainty is due to the background subtraction: using different-sized apertures for the same object introduces an error of 17, 10, 8, 8 and 10 per cent at 100, 160, 250, 350 and 500 μm, respectively. A second source of error, which is large for PACS data, is due to data recording (the repeatability of independent observations of the same source) and image making (aligning, scaling and filtering). We found it to be 20, 10, 2, 3 and 5 per cent. Finally, we include the calibration error, which is claimed to be below 5 per cent for PACS (Mueller et al. 2011) and 7 per cent for SPIRE (Swinyard et al. 2010). Taking the above three uncertainties to be independent we estimate the total uncertainties in our flux values of 27, 15, 11, 11 and 13 per cent at 100, 160, 250, 350 and 500 μm, respectively.

In Table 1, we list the Fornax bright galaxies with their names, co-ordinates, velocities, distances and flux densities in each band. Co-ordinates are obtained from centroiding the 500 μm data. The flux densities in Table 1 are as measured and do not include colour corrections (see section 5 of Davies et al. 2012). Velocities and distances have been taken from the NED. The value we have used for the distance is the mean redshift-independent distance given in NED; where available, we also include the standard deviation of the measurements. The number of measurements contributing to the mean range from 39 for NGC 1365 to just 1 for NGC 1437A and NGC 1437B. Distances are derived in a number of different ways:

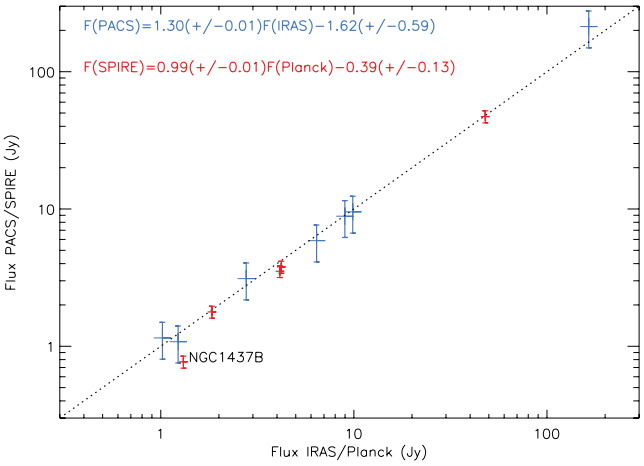

Figure 2. A comparison of *IRAS* (blue) flux densities with the PACS 100 μm and the *Planck* (red) flux densities with the SPIRE 350 μm. Linear least-squares fit parameters are given at top-left. The black dashed line is the one-to-one relationship.

primarily surface brightness fluctuations and planetary nebulae luminosity function for early type galaxies and Tully–Fisher for later types. Where required in the calibration of the method a Hubble constant of 75 km s^{-1} Mpc^{-1} has been used. Only NGC 1365 has a Cepheid distance obtained from the 'final results from the Hubble Space Telescope Key Project to measure the Hubble Constant' (Freedman et al. 2001) and this agrees with the NED mean distance of 17.9 Mpc.

For both the PACS and SPIRE data, we can make some comparisons of our results with those obtained by others. *IRAS* 100 μm fluxes are available from NED for 10 of the 11 galaxies (the exception being NGC 1437A which has not been detected at 100 μm by HeFoCS nor *IRAS*). NGC 1350 is not on the 100 μm map and we do not detect NGC 1399 or NGC 1427A (NGC 1399 is discussed in more detail in Section 3). This leaves seven galaxies that we can compare with *IRAS* as shown in Fig. 2. Individual measurements are consistent between PACS and *IRAS* within the errors, but the slope of the best-fitting line is a steep 1.3. Removing the brightest galaxy NGC 1365 ($F_{100}^{\rm PACS} = 213.06$, $F_{100}^{\rm IRAS} = 164.52$) from the sample leads to a slope of 0.95 – it is not clear from just this one galaxy whether this is a generic problem with bright sources or just specific to NGC 1365, though Aniano et al. (2012)

Table 1. The HeFoCS bright galaxy sample – (1) name, (2) and (3) position, (4) velocity, (5) distance and (6) far-infrared flux density. A dash indicates a non-detection by *Herschel* or in the case of NGC 1350, it is not observed by PACS. We estimate total uncertainties in our flux density values of 25, 15, 10, 10 and 15 per cent at 100, 160, 250, 350 and 500 μm, respectively.

(1) Name	(2) RA (J2000)	(3) Dec. (J2000)	(4) v (km s^{-1})	(5) $d_{\rm Mpc}$ (Mpc)	(6) F_{500} (Jy)	F_{350} (Jy)	F_{250} (Jy)	F_{160} (Jy)	F_{100} (Jy)
NGC 1351A	03:28:48.8	−35:10:42.2	1353	20.9 ± 1.9	0.41	0.91	1.71	2.32	1.15
NGC 1350	03:31:05.6	−33:38:27.5	1905	20.9 ± 3.6	1.51	3.78	7.15	–	–
NGC 1365	03:33:35.9	−36:08:25.9	1636	17.9 ± 2.7	17.66	47.14	106.98	205.32	213.06
NGC 1386	03:36:46.4	−35:59:57.1	868	16.2 ± 0.8	0.59	1.57	3.93	8.45	8.86
NGC 1387	03:36:56.8	−35:30:27.4	1302	17.2 ± 3.1	0.32	1.09	2.80	6.10	5.88
NGC 1399	03:38:27.0	−35:26:46.1	1429	17.9 ± 2.3	0.26	–	–	–	–
NGC 1427A	03:40:08.2	−35:37:32.5	2028	16.4 ± 0.7	0.22	0.43	0.69	1.07	–
NGC 1437A	03:43:02.7	−36:16:17.1	886	16.9	0.23	0.31	0.44	0.62	–
NGC 1436	03:43:37.0	−35:51:12.7	1387	19.1 ± 1.3	0.66	1.78	4.07	5.45	3.11
NGC 1437B	03:45:54.1	−36:21:34.6	1497	10.3	0.39	0.77	1.39	1.78	1.08
ESO358−G063	03:46:18.9	−34:56:40.9	1929	18.9 ± 4.2	1.39	3.52	7.64	12.66	9.53

Table 2. The mean luminosity and luminosity density in each band for the Virgo and Fornax bright galaxy samples. The Virgo luminosity density is that for the whole sample which lies over a distance range of 17–32 Mpc. Values in parentheses are for the sample of galaxies with distances of 17–23 Mpc (see Davies et al. 2012). The Fornax values are for the whole sample with values in parentheses with NGC 1437B, which has a somewhat discrepant distance (10.3 Mpc), removed. Errors on these values are difficult to assess because of the unknown distance errors and our definition of the cluster volume. Errors on the measured flux densities are given in the text.

Band (μm)	Mean luminosity (Virgo) $\times 10^{22}$ (W Hz^{-1} sr^{-1})	Luminosity density (Virgo) $\times 10^{-45}$ (W m^{-3} Hz^{-1})	Mean luminosity (Fornax) $\times 10^{22}$ (W Hz^{-1} sr^{-1})	Luminosity density (Fornax) $\times 10^{-45}$ (W m^{-3} Hz^{-1})
100	3.4	6.5(19.7)	9.4	24.5(39.9)
160	4.4	8.3(25.9)	8.3	25.2(40.3)
250	2.4	4.6(14.8)	4.3	14.2(23.1)
350	1.0	1.9(6.3)	1.9	6.1(9.9)
500	0.4	0.7(2.3)	0.6	2.2(3.6)

highlight a similar problem when relating PACS and *Spitzer* data. The *IRAS*/PACS colour corrections are negligible. NED gives *ISO* 150 and 170 μm flux densities of 194 and 167 Jy, respectively, for NGC 1365. The mean of these is 181 Jy which compares with our value of ∼205 Jy at 160 μm, again consistent within our calculated errors. The Planck consortium have released a point source catalogue of bright sources which, at 350 μm, contains five of the galaxies in our list. In Fig. 2, we also compare these 350 μm flux densities (we use the *Planck* GAUFLUX value for extended sources) with our SPIRE data – there is a reasonably close agreement between the SPIRE and *Planck* values, with only NGC 1437B being slightly discrepant (see Fig. 2). The SPIRE/*Planck* colour correction is small ($F_{350}^{\rm SPIRE}/F_{350}^{\rm Planck} = 0.99$) and has been ignored, Ciesla et al. (2012). For NGC 1365 we also have a *Planck* detection at 550 μm of 13.62 Jy. For a typical dust temperature of 20 K a correction of ∼1.2 is necessary to transform this to what is expected at 500 μm (Baes et al., in preparation). Carrying out this correction leads to a value of 16.34 Jy compared to 17.66 Jy measured from our SPIRE data, this value is again consistent within our quoted errors – the SED of NGC 1365 is discussed further in Section 3.

3 THE DERIVED PARAMETERS OF THE SAMPLE GALAXIES

3.1 Luminosity and luminosity density

Given the apparent shape (peaked) of the Virgo cluster luminosity distributions we decided to characterize each distribution solely by its mean values (Davies et al. 2012). With so few galaxies in this sample this is also about all we can justifiably do for Fornax. Mean values are given in Table 2, where they are also compared to Virgo. It is clear that the majority of the far-infrared energy of the cluster is being produced at the shortest of these wavelengths. The mean luminosity of galaxies in Fornax is higher than that of Virgo because of the total dominance in the far-infrared of NGC 1365. For example at 250 μm, 76 per cent of the luminosity of the cluster is produced by just this one galaxy.

For Virgo the luminosity distributions turned over at both the faint and luminous ends and so we could make an estimate of the luminosity density in each band. Based on the same assumption (we have too few Fornax galaxies to conclusively demonstrate this) we can in the same way calculate a luminosity density for Fornax. The volume sampled over 16 square degrees of sky is ∼12.9 Mpc^3 for galaxies between the extremes of distance of 10.3 and 20.9 Mpc. This seems a little large for a cluster, in which case it is the distance of NGC 1437B that is discrepant. Removing NGC 1437B from the sample the volume is ∼7.9 Mpc^3 (galaxies between 16.2 and 20.9 Mpc). Densities calculated with NGC 1437B removed from the sample will be given in parentheses after the value for the whole sample. As explained in Davies et al. (2012), Virgo cluster members in the HeViCS sample extend from 17 to 32 Mpc, which is also a large distance compared to what is normally assumed for the size of a cluster. So, all densities quoted for Virgo will be given using both the whole sample and only those with distances between 23 and 17 Mpc given in parentheses.

It is not easy to define the size of a given cluster so that realistic comparisons can be made between clusters of different sizes. Ferguson (1989b) gives the core radii of Virgo and Fornax as ≈0.6 and ≈0.3 Mpc, respectively. This is a ratio of a factor of 4 in area, just the same as the ratio of field sizes between the HeViCS and HeFoCS surveys and so we will compare cluster properties using galaxies detected in both cases over the full survey area.

Luminosity densities calculated in the above way are given in Table 2. Far-infrared luminosity densities are higher by about a factor of 3 in Fornax compared to Virgo. This is consistent with the factor of 2.5 times larger central number density of galaxies in Fornax compared to Virgo (Ferguson 1989a). Comparisons of luminosity densities with other surveys are discussed by Davies et al. (2012), but of particular interest is the Saunders et al. (1990) value for the mean local luminosity density. In the range 42.5–122.5 μm, they derive a value of 4.0×10^7 L$_\odot$ Mpc^{-3}. Using this bandpass and our 100 μm luminosity density, we can make an approximate comparison with the Saunders et al. (1990) value.[3] We calculate a value of $5.8(8.6) \times 10^9$ L$_\odot$ Mpc^{-3} for Fornax compared with $1.1(3.3) \times 10^9$ L$_\odot$ Mpc^{-3} for Virgo. The Fornax value is 145(238) times larger than the local mean value measured by *IRAS*.

The far-infrared luminosity of each galaxy can be calculated using non-overlapping bands corresponding to each *Herschel* wavelength (not necessarily centred on the nominal wavelength because of the uneven band spacing). As in Davies et al. (2012), we define the *Herschel* far-infrared luminosity as

$$L_{100-500} = 3.1 \times 10^4 d_{\rm Mpc}^2[(f_{100}\Delta f_{100}) + (f_{160}\Delta f_{160}) + (f_{250}\Delta f_{250}) + (f_{350}\Delta f_{350}) + (f_{500}\Delta f_{500})] \quad {\rm L}_\odot,$$

where $f_{100}, f_{160}, f_{250}, f_{350}, f_{500}$, $\Delta f_{100} = 18.0$, $\Delta f_{160} = 8.9$, $\Delta f_{250} = 4.6$, $\Delta f_{350} = 3.1$ and $\Delta f_{500} = 1.8$ are the flux density (Jy) and bandwidth

[3] Note that the Saunders et al. value is derived from both *IRAS* 60 and 100 μm flux densities. The 60 μm flux density in particular may be influenced by a warmer dust component associated with star formation that is not included in the fits to our data.

(10^{11} Hz) in each band, respectively, and we have taken the solar luminosity to be 3.9×10^{26} W. Calculating the luminosity in this way means that it does not depend on any particular fit to the SED, i.e. it is valid for galaxies well fitted by a single modified blackbody with any value of emissivity power index (β), those that require two components or more and those that do not have a thermal spectrum. Far-infrared luminosities ($L_{100-500}$) for each galaxy are listed in Table 3. Comparing the average far-infrared SED of the galaxies in the sample, we find that the highest flux density occurs almost equally in the 100 and 160 μm bands, with the flux density about one-third of the total in each case.

Simply multiplying the luminosity densities given in Table 2 by the bandwidths, as above, we obtain a Fornax 100–500 μm far-infrared luminosity density of $5.8(9.5) \times 10^9\,\mathrm{L}_\odot\,\mathrm{Mpc}^{-3}$ using a solar luminosity of 3.9×10^{26} W. This is a little over three times higher than the Virgo value of $1.6(7.0) \times 10^9\,\mathrm{L}_\odot\,\mathrm{Mpc}^{-3}$ (Davies et al. 2012).

In Davies et al. (2012) we define the apparent stellar luminosity from 0.4 to 2.5 μm as

$$L_{0.4-2.5} = 3.1 \times 10^7 d^2_{\mathrm{Mpc}}[(f_g \Delta f_g) + (f_r \Delta f_r) + (f_i \Delta f_i) + (f_J \Delta f_J) + (f_H \Delta f_H + (f_K \Delta f_K))] \quad \mathrm{L}_\odot,$$

where $f_g, f_r, f_i, f_J, f_H, f_K$, $\Delta f_g = 1.9$, $\Delta f_r = 1.1$, $\Delta f_i = 1.6$, $\Delta f_J = 0.9$, $\Delta f_H = 0.3$ and $\Delta f_K = 0.5$ are the flux (Jy) and bandwidth (10^{14} Hz) in each band, respectively. The g, r and i band data ($\lambda_g = 0.48$, $\lambda_r = 0.62$, $\lambda_i = 0.76$ μm) were taken from the Sloan Digital Sky Survey (SDSS). For the Fornax galaxies, we do not have SDSS data or any other uniform optical data and so we have had to rely on the near-infrared (NIR) data only. In Davies et al. (2012), we showed that about 73 per cent of the observed stellar radiation is emitted in these NIR bands and so we have multiplied the calculated stellar luminosity by a factor of 1.36 to account for this. For NGC 1427A and NGC 1437A, we do not have NIR data and so we have just used the blue-band magnitude and an absolute blue-band magnitude of the Sun of 5.45. In the NIR, the values used are from the two Micron All Sky Survey (2MASS) which lists J, H and K band (total) magnitudes ($\lambda_J = 1.25$, $\lambda_H = 1.65$, $\lambda_K = 2.17$ μm). The 2MASS website gives the following zero-points for the conversion of magnitudes to Jy: $K_J = 8.01$, $K_H = 7.53$, $K_K = 7.06$.

Summing the contribution from all the galaxies leads to an optical luminosity density of $\rho_{0.4-2.5} = 8.6(14.1) \times 10^9\,\mathrm{L}_\odot\,\mathrm{Mpc}^{-3}$ just 1.5 times larger than the far-infrared value given above. The optical luminosity (uncorrected for extinction) is found to be about three times that of the far-infrared in Virgo (Davies et al. 2012).

The optical and far-infrared luminosities can be used to make a crude estimate of the 'typical' optical depth ($\langle\tau\rangle$) experienced by a photon as it leaves a galaxy, based on a simple screen of dust model:

$$\langle\tau\rangle = \ln\left(1.0 + \frac{L_{100-500}}{L_{0.4-2.5}}\right).$$

Values of $\langle\tau\rangle$ are listed in Table 3. The mean value for galaxies in this sample is $\langle\tau\rangle_{\mathrm{mean}} = 0.4 \pm 0.1$ so on average the optical energy is emerging from regions of intermediate optical depth (neither totally optically thin or thick) – the mean value found for Virgo was just the same. Individual values of $\langle\tau\rangle$ also have a similar range to Virgo of 0.06–1.10. Interestingly NGC 1365, the brightest far-infrared source in both Virgo and Fornax, has a far-infrared luminosity almost the same as its optical luminosity, and the typical photon originates from an optically thick ($\tau = 1.11$) region. As pointed out in Davies et al. (2012), the two 'optically thick' galaxies with $\langle\tau\rangle$ greater than unity in the Virgo sample are both relatively face-on late-type spirals – NGC 4234 (Sc) and NGC 4299 (Scd); this is also now true for Fornax (inclinations to the plane of the sky are 56°, 40° and 20° for NGC 1365, NGC 4234 and NGC 4299, respectively). As galactic dust is typically confined to a relatively thin disc, the value of τ should be dependent on the inclination of each galaxy to the line of sight. It is therefore surprising that the highest values of τ are associated with relatively face-on galaxies. The above value of $\langle\tau\rangle_{\mathrm{mean}}$ is very close to the value given in Saunders et al. (1990) derived in a similar way using *IRAS* data ($\langle\tau\rangle^{\mathrm{IRAS}}_{\mathrm{mean}} = 0.3 \pm 0.1$). The value we find implies that on average ∼33 per cent of the stellar radiation of a galaxy is absorbed by dust. The value is in agreement with what was found by Popescu & Tuffs (2002) using a sample of late-type Virgo galaxies observed with *ISO*.

3.2 Dust mass and temperature

In order to derive dust mass and temperature, we have fitted the SED of each galaxy, as defined by the flux densities given in Table 1, with

Table 3. The Fornax Cluster Survey bright galaxy Sample – (1) name, (2) absolute B magnitude, (3) stellar mass, (4) H I mass, (5) dust mass, (6) dust temperature, (7) stellar luminosity from 0.4 to 2.5 μm, (8) far-infrared luminosity from 100 to 500 μm, (9) mean optical depth, (10) stellar to atomic gas mass ratio and (11) atomic gas to dust mass ratio. Optical and near-infrared magnitudes where required are taken from the NED data base. NGC 1427A and NGC 1437A were not detected by 2MASS and so their stellar mass has been calculated using just their B-band magnitude and an absolute magnitude of the Sun of $\mathrm{M}^B{}_\odot = 5.47$ (for the same reason they do not have an integrated optical luminosity). NGC 1399 only has a measurement at 500 μm and so we are not able to calculate a dust mass. The early type galaxies NGC 1386, NGC 1387 and NGC 1399 have not been detected at 21 cm.

(1) Name	(2) M_B	(3) Log(M_{Stars}) ($\mathrm{M}_\odot$)	(4) Log($M_{\mathrm{H\,I}}$) ($\mathrm{M}_\odot$)	(5) Log(M_{Dust}) ($\mathrm{M}_\odot$)	(6) T_{d} (K)	(7) Log($L_{0.4-2.5}$) ($\mathrm{L}_\odot$)	(8) Log($L_{100-500}$) ($\mathrm{L}_\odot$)	(9) $\langle\tau\rangle$	(10) $M_{\mathrm{Stars}}/M_{\mathrm{H\,I}}$	(11) $M_{\mathrm{H\,I}}/M_{\mathrm{Dust}}$
NGC 1351A	−17.39	9.41	8.80	7.04 ± 0.07	17.1 ± 1.1	8.93	8.85	0.61	4.1	57.5
NGC 1350	−20.44	10.71	9.15	7.68 ± 0.15	16.8 ± 2.0	10.26	–	–	36.3	29.5
NGC 1365	−21.03	10.87	10.08	8.35 ± 0.07	22.0 ± 2.6	10.50	10.80	1.10	6.2	53.7
NGC 1386	−18.96	10.24	–	6.73 ± 0.07	23.6 ± 2.8	9.76	9.33	0.32	–	–
NGC 1387	−19.50	10.55	–	6.58 ± 0.07	24.2 ± 2.3	10.00	9.20	0.15	–	–
NGC 1399	−20.71	11.05	–	–	–	10.55	–	–	–	–
NGC 1427A	−17.63	9.23	9.18	6.54 ± 0.10	16.4 ± 1.8	9.23	8.08	0.09	1.1	436.5
NGC 1437A	−17.23	9.07	8.70	6.56 ± 0.13	14.8 ±	9.07	7.89	0.06	2.3	138.0
NGC 1436	−19.00	10.00	8.17	7.18 ± 0.07	18.5 ± 1.2	9.54	9.15	0.35	67.6	9.8
NGC 1437B	−16.08	8.85	8.08	6.56 ± 0.08	14.6 ± 1.0	8.29	8.15	0.55	5.9	33.1
ESO358−G063	−18.78	9.91	9.26	7.38 ± 0.07	19.8 ± 1.3	9.45	9.49	0.74	4.5	75.9

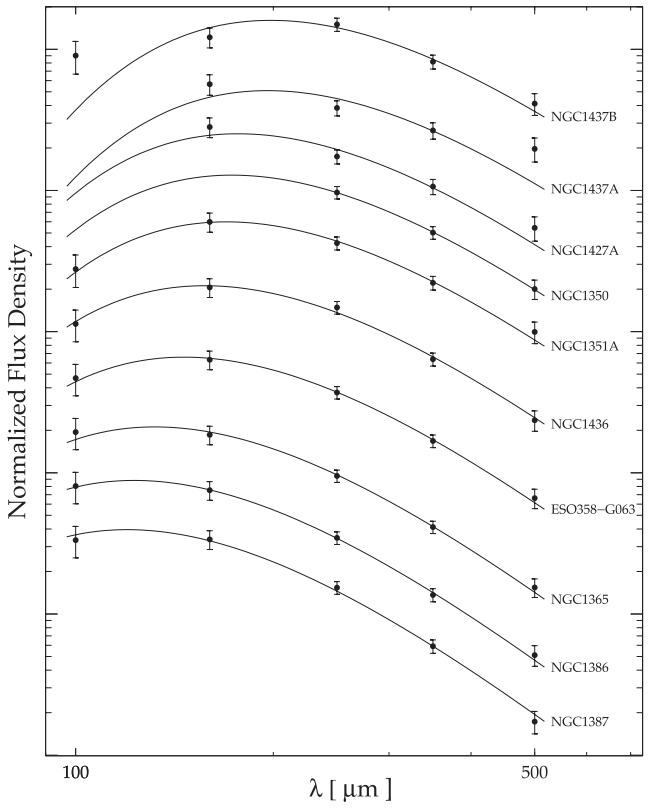

Figure 3. *Herschel* SEDs of the Fornax bright galaxy sample. The SEDs are ordered with the coldest galaxy at the top.

a single temperature modified blackbody. The method is identical to that used for the Virgo galaxies and is fully described in Davies et al. (2012). In summary, we use a power-law dust emissivity $\kappa_\lambda = \kappa_0(\lambda_0/\lambda)^\beta$, with spectral index $\beta = 2$ and emissivity $\kappa_0 = 0.192$ m^2 kg^{-1} at $\lambda_0 = 350\,\mu$m. The monochromatic flux densities measured from the images, as reported in Table 1, come from the pipeline calibration. They have been derived from the passband-weighted flux density (measured by the instruments), applying a colour correction for a flat energy spectrum ($F_\nu \propto \nu^{-1}$). When doing the fit to the data points, we first remove this correction and then apply our own colour correction to the pipeline monochromatic fluxes densities. The colour corrections are given in table 3 of Davies et al. (2012). The model fit to the data was obtained with a standard χ^2 minimization technique.

Plotting the data given in Table 1 shows that the majority of galaxies are simply and well fitted by this single temperature-modified blackbody curve with fixed emissivity index; the fits are shown in Fig. 3 (ordered by increasing temperature). This good correspondence of the data with a single modified blackbody curve is essentially the same result we obtained for Virgo (Davies et al. 2012; see also Boselli et al. 2012; Dale et al. 2012). The most notable discrepant point is that at 100 μm for NGC 1437B. As with many Fornax galaxies when compared to Virgo, there is no literature discussion of NGC 1437B that we can find. It is described as an I0 galaxy in NED and as an edge-on Sd in Thomas et al. (2008). There is a *GALEX* image that shows that there is star formation in bright 'clumps' and it clearly looks as though it has been disturbed in some way by the local environment. Presumably the excess 100 μm emission is due to warm dust heated by this on-going star formation. NGC 1427A and NGC 1437A both have what might be excess emission at 500 μm, but it is difficult to be sure because there are only four data points and the modified blackbody fit is not so good. Note that NGC 1399 is omitted from Fig. 3 because we only have one flux density measurement at 500 μm.

Derived dust masses and temperatures are in the range $10^{6.54-8.35}$ M$_\odot$ and 14.6–24.2 K, respectively ($10^{6.22-8.17}$ M$_\odot$ and 12.8–27.2 K for Virgo). Prior to the availability of observations at wavelengths longer than about 100 μm, calculated galaxy dust masses and temperatures from surveys similar to HeViCS and HeFoCS were typically $10^{6.6}$ M$_\odot$ and 30–50 K, respectively (taken from Soifer et al. 1987 where they have 31 galaxies in common with HeViCS; see also Devereux & Young 1990). This confirms the need for longer wavelength observations ($\lambda > 160\,\mu$m) to sample the Rayleigh–Jeans tail of the SED and detect the colder dust component in galaxies.

3.3 Stellar mass

We have calculated stellar masses ($M_{\rm Star}$) for each galaxy (Table 3) using the prescription given in Bell et al. (2003), i.e.

$$\log M_{\rm star} = -0.359 + 0.21(B - V) + \log \frac{L_H}{\rm L_\odot},$$

where L_H has been calculated using an H-band absolute magnitude for the Sun of $\rm M_H^\odot = 3.32$. M_H and $(B - v)$ values have been taken from NED. Because of the lack of data, for NGC 1427A and NGC 1437A the stellar masses have been calculated solely from their B-band magnitudes using a B-band magnitude for the Sun of $\rm M_B^\odot = 5.47$.

3.4 Gas mass

Where available (8 out of 11 galaxies), we have taken the 21 cm spectral line flux integral ($S_{\rm Tot}$, Jy km s^{-1}) for each galaxy from NED and used the distances given in Table 1 to obtain atomic hydrogen gas masses ($M_{\rm HI}$, M$_\odot$). The masses have been obtained using the standard formula

$$M_{\rm HI} = 2.4 \times 10^5 d^2_{\rm Mpc} S_{\rm Tot}.$$

Atomic hydrogen gas masses are given in Table 3 along with dust and stellar mass.

Derived from CO observations there are four detections and three upper limits on the molecular hydrogen masses of these galaxies (Horellou, Casoli & Dupraz 1995). NC1365, NGC 1386, NGC 1436 and ESO358-G063 have Log($M_{\rm H_2}$) equal to 10.3, 8.3, 7.7 and 8.6, respectively. There is almost a factor of 2 more molecular hydrogen in NGC 1365 than atomic, and NGC 1386 is surprisingly detected in CO, but not H I. NGC 1351A, NGC 1350 and NGC 1387 all have upper limits on their molecular gas masses that are in each case more than a factor of 10 less than their atomic hydrogen masses. We have not incorporated this molecular gas data into Table 3 or discussed it further, so this paper is directly comparable with the equivalent paper on Virgo, where we have not included molecular gas masses (Davies et al. 2012). In the above, we have taken $X_{\rm CO} = 3 \times 10^{20}$ cm^2 (K km s^{-1})$^{-1}$.

3.5 Mass densities

By simply dividing the total mass in each component by the volume sampled [$\sim$12.9(7.2) Mpc^3], we can calculate the cluster mass densities. Provided the luminosity distributions in each far-infrared band are peaked, the total cluster dust mass should be well constrained by our sample galaxies unless there is a significant dust

Table 4. The mass densities in stars, gas and dust in the Fornax and Virgo clusters along with that for the local field, represent when compared to the local field. The Virgo values are for the whole sample, which lies over a distance range of 17–32 Mpc. Values in parentheses are for the sample of galaxies with distances of 17–23 Mpc (see Davies et al. 2012). The Fornax values are for the whole sample with values in parentheses with NGC 1437B, which has a somewhat discrepant distance (10.3 Mpc), removed. References for the field values are given in the text. The final two columns give the overdensities of Virgo and Fornax compared to the field value.

	Virgo ($M_\odot$ Mpc^{-3})	Fornax ($M_\odot$ Mpc^{-3})	Field ($M_\odot$ Mpc^{-3})	Virgo overdensity	Fornax overdensity
Stars	$7.8(29.7) \times 10^9$	$24.0(39.2) \times 10^9$	$0.2 \pm 0.1 \times 10^9$	34(129)	120(195)
Gas	$0.5(1.4) \times 10^9$	$1.4(2.3) \times 10^9$	$0.08 \pm 0.01 \times 10^9$	6(18)	18(29)
Dust	$8.6(27.8) \times 10^6$	$26.5(43.3) \times 10^6$	$0.22 \pm 0.04 \times 10^6$	39(126)	120(196)

component in the intergalactic medium. From the dust in our sample galaxies, we derive the densities given in Table 4. Values for Virgo have been taken from Davies et al. (2012). These values can be compared with a recent determination of the local dust mass density for galaxies in all environments from Dunne et al. (2011). This shows that Fornax is overdense in dust by about a factor of 120(196) while Virgo is overdense by about a factor of 39(126).

If the Fornax H I mass function is peaked, similar to Virgo (Davies et al. 2004; Taylor 2010), the H I gas in these galaxies should provide a good estimate of the cluster total. Using the eight H I masses available (Table 3), we derive the H I mass density shown in Table 4. The value for Virgo is taken from Davies et al. (2012). Recently, Davies et al. (2011) measured a local 'field' H I mass density of $7.9 \pm 1.2 \times 10^7$ $M_\odot$ Mpc^{-3} (see also Martin et al. 2010). Thus, the Fornax cluster is overdense in H I, when compared to the field, by a factor of 18(29) and Virgo by 6(18).

As a check of our assumption that our sample galaxies contain the majority of H I in the volume, we have looked at the HIPASS data for Fornax as described in Waugh (2002). There are three galaxies in our *Herschel* field that have H I detections by Waugh, but are not in our sample (a visual inspection shows that they are all detected in the far-infrared, but not at the required flux level). The three H I detections are ESO358-G015, ESO358-G051 and ESO358-G060 and using their distances as listed in NED they amount to just 9 per cent of the total atomic hydrogen in our sample galaxies.

Comparing stellar mass functions is not quite so straightforward because of uncertainties in the faint end slope of the cluster luminosity function, i.e. the numbers of faint dwarf galaxies (see Sabatini et al. 2003 and references therein). For the stars in our sample galaxies, we obtain the densities given in Table 4. The Virgo value is again taken from Davies et al. (2012). Baldry, Glazebrook & Driver (2008) recently derived the local galaxy stellar mass function and from it the field stellar mass density (Table 4). Thus, the Fornax cluster is overdense in stars by 120(195) compared to values for Virgo of 34(129). Where required in the above derivations we have used $H_0 = 72\,\mathrm{km\,s^{-1}}$, $\Omega_\mathrm{m} = 0.27$ and $\Omega_\Lambda = 0.73$.

The larger stellar mass density we calculate for Fornax compared to Virgo is again roughly consistent with the factor of 2.5 higher number density of galaxies derived by Ferguson (1989a) – Fornax is a higher overdensity than Virgo. Interestingly, both Virgo and Fornax represent about equal overdensities of dust and stars, but the atomic gas is relatively much more depleted (Table 4). This presumably indicates that atomic gas has been removed from these galaxies without the loss of consummate amounts of dust, though Cortese et al. (2010) show, by the clear truncation of Virgo cluster dust discs, that some dust must be lost from the outer regions of galaxies in the cluster environment.

We can make a simple calculation to see the effect of ram pressure on both the gas and the dust. The force per unit area a particle in the disc of a galaxy experiences is the difference between the ram pressure and the restoring force per unit area due to the discs surface mass density (Gunn & Gott 1972). In this case the acceleration a particle undergoes depends on its cross-sectional area (a) and its mass (m_p) and for constant acceleration the time-scale for removal is just proportional to $\sqrt{m_\mathrm{p}/a}$. Using typical values for the masses ($m_\mathrm{g} \approx 10^{-27}$, $m_\mathrm{d} \approx 10^{-14}$) and sizes ($a_\mathrm{g} \approx 10^{-20}$, $a_\mathrm{d} \approx 10^{-12}$) of gas and dust particles leads a time-scale for dust removal about a factor of 100–1000 longer than gas removal (this ignores viscous drag between the gas and dust; see Davies et al. 1998). Evidence from Virgo shows that atomic and molecular gas are also affected very differently by the cluster environment. There is no evidence for an H_2 deficiency in Virgo but there clearly is an atomic gas deficiency (Gavazzi et al. 2008; Young et al. 2011). So, a complementary explanation for the non-removal of dust is that it is primarily associated with dense H_2 reservoirs that are very resistant to the ram pressure stripping process.

Using the Davies et al. (2010) and Dunne et al. (2011) values for the global H I and dust mass densities gives a local 'field' atomic gas to dust ratio of 363,[4] while the same ratio in the Fornax and Virgo clusters is 52(53) and 58(50), respectively. From the above it seems that these low values are entirely due to the loss of atomic gas. In each case this amounts to about six times as much H I lost from these galaxies as is presently contained within them (5×10^{11} and 1×10^{11} $M_\odot$, respectively, for Virgo and Fornax). It seems that irrespective of the different environments prevalent in these two clusters the atomic gas loss mechanisms are equally effective. H I complexes within the Virgo cluster, but external to previously identified galaxies, have been found by Davies et al. (2004), Oosterloo & van Gorkom (2005) and Kent et al. (2007), but they only represent a small fraction of the cluster atomic gas.

3.6 The spectral energy distribution of NGC 1365

The brightest Virgo cluster galaxy at these wavelengths is NGC 4254 ($F_{100} = 114.2$ Jy, $D = 17$ Mpc; Davies et al. 2012), but this is totally outshone by the Fornax cluster galaxy NGC 1365 ($F_{100} = 213.5$ Jy, $D = 17.9$ Mpc). Being so bright NGC 1365 is also detected by *Planck* in four bands at 350, 550, 850 and 1382 μm. In Fig. 4, we show the PACS, SPIRE and *Planck* data along with the best-fitting modified blackbody taken from Fig. 3. The *Planck* data are

[4] The local value of the gas-to-dust ratio for the Milky Way is ∼143 (Draine et al. 2007), but our calculation neglects the molecular gas included in this value.

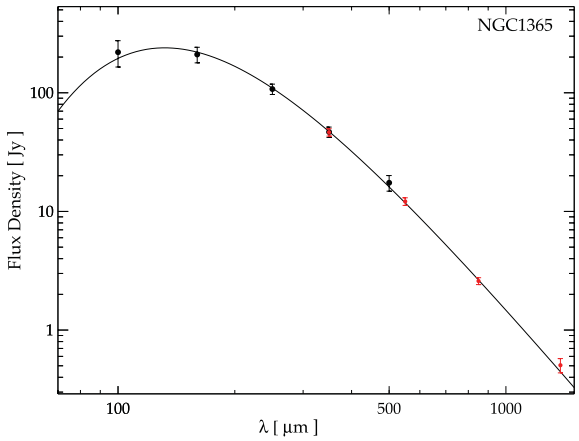

Figure 4. The far-infrared SED of NGC 1365. Black points are the PACS and SPIRE data and the black line the best modified blackbody curve fit to them. The red points are the *Planck* data.

those derived by fitting a 2D Gaussian to the data (GAUFLUX, which should be more appropriate for extended sources) and colour corrected using the *Herschel* SED and the tables in the explanatory notes of the *Planck* early release compact source catalogue. The *Planck* data fit remarkably well the modified blackbody all the way out to 1382 μm. There is no significant sign of any excess emission above that of the modified blackbody, with the point at 1382 μm being the most discrepant.

The band centred on 1382 μm contains the CO(2–1) line and this might explain the slight excess. According to Sandqvist, Joersaeter & Lindblad (1995) the total CO(1–0) luminosity of NGC 1365 is 5200 Jy km s^{-1}. For the *Planck* bandwidth (33 per cent of the central frequency) and using the measured CO(2–1)/CO(1–0) = 0.8 ratio we find that the CO(2–1) line contributes 0.045 Jy (7 per cent of the total) to the 1382 μm flux density. If this is subtracted from the colour-corrected data, then the 1382 μm point sits nicely on top of the modified blackbody curve.

Over these longer, *Planck* wavelengths, we might also expect an additional contribution to the observed flux density from free–free emission (synchrotron emission only starts to become important at wavelengths greater than ∼1 cm; Condon 1992). Combining equations 23 and 26 from Condon (1992) we get

$$\left(\frac{F_\lambda}{\mathrm{Jy}}\right) = 1.2\times10^{-10}\left(\frac{\lambda}{\mu\mathrm{m}}\right)^{0.1}\left(\frac{d_{\mathrm{Mpc}}}{\mathrm{Mpc}}\right)^{-2}\left(\frac{L_{\mathrm{FIR}}}{\mathrm{L}_\odot}\right),$$

where F_λ is the free–free flux density in Jy at wavelength λ in μm, d_{Mpc} is the distance in Mpc and L_{FIR} the far-infrared luminosity in solar units. For NGC 1365 at a distance of $d_{\mathrm{Mpc}} = 17.9$ Mpc and $L_{\mathrm{FIR}} = L_{100-500} = 6.5\times10^{10}\,\mathrm{L}_\odot$, the predicted flux densities at 850 and 1382 μm are 0.048 and 0.050 Jy, respectively. These values are again much smaller than the extrapolation of the modified blackbody curve and so free–free emission is predicted to be only a small fraction of the emission at these wavelengths.

NGC 1365 is a powerful Seyfert (type 1.8) galaxy (Veron-Cetty & Veron 2006), but no sign of the active galactic nucleus is seen in its global far-infrared/sub-mm spectrum. Previous observations of some more passive galaxies has revealed an excess at wavelengths beyond 350 μm, particularly the Milky Way (Leitch et al. 1997) and star-forming dwarf galaxies (Grossi et al. 2010). This emission has been associated with an additional 'spinning dust' component (Draine & Lazarian 1998a,b), but it is not observed here.

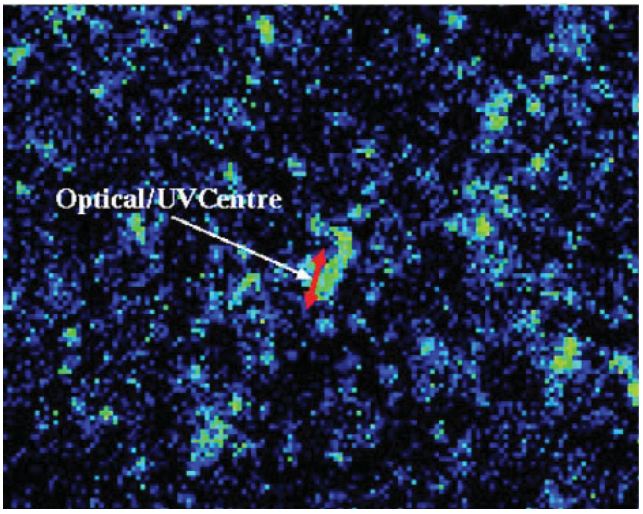

Figure 5. A part of the 500 μm image (radius ∼22.5 arcmin) centred on the position of NGC 1399. Extended emission is seen at approximately the position of NGC 1399. The red arrow shows approximately the position, extent and orientation of the radio jet. The centre of the galaxy when measured in the optical and ultraviolet is indicated by the white arrow.

3.7 Emission from NGC 1399

With a *B*-band absolute magnitude of −20.7, NGC 1399 is just about a typical (L^*) galaxy in terms of its optical luminosity. But, being an elliptical galaxy (E1) lying at the very heart of the cluster we might expect that NGC 1399's interstellar medium is somewhat depleted compared to a galaxy like the Milky Way. No atomic hydrogen has been detected in NGC 1399, though there have been previous detections in the far-infrared possibly associated with dust emission. There is an *IRAS* detection at 0.3 Jy (NED) which would be a marginal detection in our data dependent on the size of the source – but we detect nothing. There is a *Spitzer* (MIPS) detection at 160 μm of 0.026 Jy (Temi, Brighenti & Matthews 2009), but this is below our detection limit. For the similar, though slightly brighter in the optical M87, our observations gave detections in all the PACS/SPIRE bands (Davies et al. 2012), though this was almost exclusively synchrotron emission and not thermal emission from dust (Baes et al. 2010). For synchrotron emission from NGC 1399, we expect the highest flux density at the longest wavelengths, consistent with our detection at 500 μm and our non-detection at 100 μm. For the same spectral slope as M87[5] we would expect a 100 μm flux density of about 0.1 Jy, below our detection threshold and rather at odds with the *IRAS* 100 μm detection (which is too high) and similarly at odds with the MIPS measurement (which would be too low).

There are radio synthesis observations (44 arcsec resolution) of NGC 1399 at 35 cm that clearly show two opposing radio jets emanating from the nucleus (Jones & McAdams 1992). In Fig. 5, we show the 500 μm image of NGC 1399 with the position and extent of the 35 cm radio jet indicated by the red arrow. The 500 μm emission appears more extended than the jet and also the jet seems to be off-set from it, but roughly at the same position angle. The optical centre of the galaxy (NED) corresponds with the centre of the jet. For M87 the far-infrared emission clearly traces the radio

[5] There are actually 10 radio flux densities for NGC 1399 listed in NED, but there is a large scatter in the values with as much as a factor of 7 difference at the same frequency, so we have not used this data to derive a spectral slope.

jet and so it is a bit of a puzzle as to why NGC 1399 is different. If the emission is actually due to dust, and this is some form of dust lane, then it is strange that it is not detected more strongly in the other SPIRE bands. It also extends over some 3 arcmin (16 kpc) – this is large for a dust feature in an elliptical galaxy – NGC 1399 does not appear in the catalogue of dusty ellipticals (Ebneter & Balick 1985). There is also the possibility that this is some chance alignment of background sources. The region shown in Fig. 5 is some 20 arcmin across, specifically made this large to illustrate the brightness and number density of sources across the field. There are background sources that could conspire to produce the emission we are associating with NGC 1399, and so at the moment the origin of this 500 μm emission is not clear.

4 SUMMARY

In this paper, we have described the HeFoCS and far-infrared observations of 11 bright cluster galaxies. We carry out aperture photometry and show that our measurements are consistent with previous data where available. For 10 of the 11 galaxies, we fit SED and derive dust masses and temperatures. We combine dust masses with star and gas masses from the literature to assess the global properties of the galaxies in our sample. These global properties are similar to those detected by us in the Virgo cluster (HeViCS; Davies et al. 2012). We have then compared Fornax and Virgo with each other and the field. Generally, Fornax is more dense in stars, gas and dust by a factor of 3–4 relative to Virgo. When compared to the lower density local field of galaxies, Fornax is overdense by a factor of about 120 in stars and dust, but only a factor of 18 in gas. Values for Virgo are about 34 and 39 for stars and dust, reducing to 6 for gas. Both the Fornax and Virgo clusters are relatively depleted in gas to the same extent – gas loss does not seem to be dependent on these two different galactic environments. We specifically discuss two of the sample galaxies in more detail. NGC 1365 because it is the brightest far-infrared galaxy in Virgo and Fornax combined. NGC 1399 because it is only detected at the longest wavelength of 500 μm.

ACKNOWLEDGMENTS

The *Herschel* spacecraft was designed, built, tested and launched under a contract to ESA managed by the *Herschel*/*Planck* Project team by an industrial consortium under the overall responsibility of the prime contractor Thales Alenia Space (Cannes), and including Astrium (Friedrichshafen) responsible for the payload module and for system testing at spacecraft level, Thales Alenia Space (Turin) responsible for the service module and Astrium (Toulouse) responsible for the telescope, with in excess of a hundred sub-contractors.

PACS has been developed by a consortium of institutes led by MPE (Germany) and including UVIE (Austria); KU Leuven, CSL, IMEC (Belgium); CEA, LAM (France); MPIA (Germany); INAF-IFSI/OAA/OAP/OAT, LENS, SISSA (Italy); IAC (Spain). This development has been supported by the funding agencies BMVIT (Austria), ESA-PRODEX (Belgium), CEA/CNES (France), DLR (Germany), ASI/INAF (Italy) and CICYT/MCYT (Spain).

SPIRE has been developed by a consortium of institutes led by Cardiff University (UK) and including Univ. Lethbridge (Canada); NAOC (China); CEA, LAM (France); IFSI, Univ. Padua (Italy); IAC (Spain); Stockholm Observatory (Sweden); Imperial College London, RAL, UCL-MSSL, UKATC, Univ. Sussex (UK) and Caltech, JPL, NHSC, Univ. Colorado (USA). This development has been supported by national funding agencies: CSA (Canada); NAOC (China); CEA, CNES, CNRS (France); ASI (Italy); MCINN (Spain); SNSB (Sweden); STFC (UK) and NASA (USA).

This research has made use of the NASA/IPAC Extragalactic Database (NED) which is operated by the Jet Propulsion Laboratory, California Institute of Technology, under contract with the National Aeronautics and Space Administration.

This publication makes use of data products from the 2MASS, which is a joint project of the University of Massachusetts and the Infrared Processing and Analysis Center/California Institute of Technology, funded by the National Aeronautics and Space Administration and the National Science Foundation.

The development of *Planck* has been supported by: ESA; CNES and CNRS/INSU-IN2P3-INP (France); ASI, CNR, and INAF (Italy); NASA and DoE (USA); STFC and UKSA (UK); CSIC, MICINN and JA (Spain); Tekes, AoF and CSC (Finland); DLR and MPG (Germany); CSA (Canada); DTU Space (Denmark); SER/SSO (Switzerland); RCN (Norway); SFI (Ireland); FCT/MCTES (Portugal) and PRACE (EU).

SB, LH and SDA acknowledge financial support by ASI through the ASI-INAF grant 'HeViCS: the *Herschel* Virgo Cluster Survey' I/009/10/0.

This work received support from the ALMA-CONICYT Fund for the Development of Chilean Astronomy (Project 31090013) and from the Center of Excellence in Astrophysics and Associated Technologies (PBF 06).

PS is a NWO/Veni fellow.

REFERENCES

Aniano G. et al., 2012, ApJ, in press (arXiv:1207.4186)
Auld R. et al., 2012, MNRAS, in press (doi:10.1093/mnras/sts125)
Baes M. et al., 2010, A&A, 518, 53
Baldry K., Glazebrook K., Driver S., 2008, MNRAS, 388, 945
Bell E., McIntosh Daniel H., Katz N., Weinberg M., 2003, ApJS, 149, 289
Bertin E., Arnouts S., 1996, A&ASS, 117, 393
Binggeli B. et al., 1985, AJ, 90, 1681
Boselli A., Gavazzi G., 2006, PASP, 118, 517
Boselli A. et al., 2010, A&A, 518, 61
Boselli A. et al., 2012, A&A, 540, 54
Ciesla L. et al., 2012, A&A, 543, 161
Clemens M. et al., 2010, A&A, 518, 50
Condon J., 1992, ARA&A, 30, 575
Corbelli E. et al., 2012, A&A, 542, A32
Cortese L. et al., 2010, A&A, 518, 49
Dale D. et al., 2012, ApJ, 745, 95
Davies J., Alton P., Bianchi S., Trewhella M., 1998, MNRAS, 300, 1006
Davies J. et al., 2004, MNRAS, 349, 922
Davies J. et al., 2010, A&A, 518, 48
Davies J. et al., 2011, MNRAS, 415, 1883
Davies J. et al., 2012, MNRAS, 419, 3505
de Looze I. et al., 2010, A&A, 518, 54
Devereux N., Young J., 1990, ApJ, 359, 42
Dowell C. et al., 2010, Proc. SPIE, 7731, 773136
Doyon R., Joseph R., 1989, MNRAS, 239, 347
Draine B., Lazarian A., 1998a, ApJ, 494, L19
Draine B., Lazarian A., 1998b, ApJ, 508, 157
Draine B. et al., 2007, ApJ, 663, 866
Drinkwater M. et al., 1999, ApJ, 511, 97
Drinkwater M., Gregg M., Colless M., 2001, ApJ, 548, 139
Dunne L. et al., 2011, MNRAS, 417, 1510
Ebneter K., Balick B., 1985, AJ, 90, 183
Ferguson H., 1989a, AJ, 98, 36
Ferguson H., 1989b, Ap&SS, 157, 227
Freedman W. et al., 2001, ApJ, 553, 47
Gavazzi G. et al., 2008, A&A, 482, 43

Griffin M. et al., 2009, EAS, 34, 33G
Griffin M. et al., 2010, A&A, 518, 3
Grossi M. et al., 2010, A&A, 518, 52
Gunn J., Gott R., 1972, ApJ, 176, 1
Horellou C., Casoli F., Dupraz C., 1995, A&A, 303, 361
Jones P., McAdam W., 1992, ApJS, 80, 137
Jordan C. et al., 2007, ApJS, 169, 213
Kent B. et al., 2007, ApJ, 665, 15
Leitch E. et al., 1997, ApJ, 486, L23
Magrini L. et al., 2011, A&A, 535, 13
Martin A., Papastergis E., Giovanelli R., Haynes M., Springob C., Stierwalt S., 2010, ApJ, 723, 1359
Mueller T., Nielbock M., Balog Z., Klaas U., Vilenius E., 2011, PACS Photometer – Point-Source Flux Calibration PACS Herschel document PICC-ME-TN-037, v. 1.0 (2011 April 12)
Oosterloo T., van Gorkom, 2005, A&A, 437, 19
Ott S., 2010, in Mizumoto Y., Morita K., Ohishi M., eds, Astronomical data analysis systems, ASP Conf. Ser. Vol. 434, Astron. Soc. Pac., San Francisco, p. 139
Paolillo M. et al., 2002, ApJ, 565, 883
Pappalardo C. et al., 2012, A&A, 545, 75
Pilbratt G. et al., 2010, A&A, 518, 1
Poglitsch A. et al., 2010, A&A, 518, 2
Popescu C., Tuffs R., 2002, MNRAS, 567, 221
Roussel H., 2012, arXiv:1205.2576
Sabatini S. et al., 2003, MNRAS, 341, 981
Sandqvist A., Joersaeter S., Lindblad P., 1995, A&A, 295, 585
Saunders W. et al., 1990, MNRAS, 242, 318
Scharf C. A., Zurek D. R., Bureau D., 2005, ApJ, 633, 154
Schindler S., Binggeli B., Bohringer H., 1999, A&A, 343, 420
Smith M. et al., 2010, A&A, 518, 51
Soifer B. et al., 1987, ApJ, 320, 238
Swinyard B. et al., 2010, A&A, 518, 4
Taylor R., 2010, PhD thesis, Cardiff Univ.
Temi P., Brighenti F., Matthews W., 2009, ApJ, 707, 890
Thomas P., Drinkwater M., Evtigneeva E., 2008, MNRAS, 389, 102
Tuffs R. et al., 2002, ApJS, 139, 37
Veron-Cetty M., Veron P., 2006, A&A, 455, 773
Waugh M. et al., 2002, MNRAS, 337, 641
Young L. et al., 2011, MNRAS, 414, 940

This paper has been typeset from a TEX/LATEX file prepared by the author.